# Limited-angle Multi-energy CT using Joint Clustering Prior and Sparsity Regularization

Huayu Zhang[a,b] and Yuxiang Xing[a]

[a]Department of Engineering Physics, Tsinghua University and Key Laboratory of Particle & Radiation Imaging (Tsinghua University), Ministry of Education, 100084, Beijing, China.
[b]Department of Electrical and Computer Engineering, University of Wisconsin Madison, Madison, USA

## ABSTRACT

In this article, we present an easy-to-implement Multi-energy CT scanning strategy and a corresponding reconstruction method, which facilitate spectral CT imaging by improving the data efficiency the number-of-energy-channel fold without introducing visible limited-angle artifacts caused by reducing projection views. Leveraging the structure coherence at different energies, we first pre-reconstruct a prior structure information image using projection data from all energy channels. Then, we perform a k-means clustering on the prior image to generate a sparse dictionary representation for the image, which severs as a structure information constraint. We combine this constraint with conventional compressed sensing method and proposed a new model which we referred as Joint Clustering Prior and Sparsity Regularization (CPSR). CPSR is a convex problem and we solve it by Alternating Direction Method of Multipliers (ADMM).

We verify our CPSR reconstruction method with a numerical simulation experiment. A dental phantom with complicate structures of teeth and soft tissues is used. X-ray beams from three spectra of different peak energies (120kVp, 90kVp, 60kVp) irradiate the phantom to form tri-energy projections. Projection data covering only 75° from each energy spectrum are collected for reconstruction. Independent reconstruction for each energy will cause severe limited-angle artifacts even with the help of compressed sensing approaches. Our CPSR provides us with images free of the limited-angle artifact. All edge details are well preserved in our experimental study.

**Keywords:** Image reconstruction, Limited angle, Multi-energy CT, prior, sparsity, clustering

## 1. INTRODUCTION

Multi-energy CT (MECT) has become increasingly popular due to its ability to differentiate materials.[1–4] It has wide applications in the field of medical imaging, non-destructive testing and public security inspection. Many works have been published on differentiating tissue types and multiple materials,[5,6] as well as improving the contrast-to-noise ratio of reconstructions.[7] For example, MECT provides us a great tool to extracting the veins and kidney stones,[4] to quantitatively detect chemical elements such as iodine and barium.[8]

There are different dual-energy CT designs in the field: dual source, dual detector layer, kVp switching. Obviously, they acquire two sets of projection data, one for low energy and the other for high energy. With these system configurations, tri-energy or quadro-energy becomes too difficult ( or expensive ) to realize. Here, by saying projections from one energy, we mean projection from an either wide or narrow X-ray spectrum more precisely. The same terminology will be used from now on in this work. In these days, with the technology of pixelated photon counting detectors, projections from more ($> 2$) energy channels becomes an accessible choice for us. However, it is very expensive for large field-of-view imaging and has to trade off among counting rate, detector bin size, and etc. Besides these pros and cons, all these MECT systems collect data equivalent to

Further author information: Send correspondence to Yuxiang Xing
Huayu Zhang was in the department of engineering physics, Tsinghua university and now is in the department of electrical and computer engineering, university of Wisconsin Madison. E-mail: zhuayu@wisc.edu, Telephone: 1 608 770 1803
Yuxiang Xing: E-mail: xingyx@mail.tsinghua.edu.cn, Telephone: +86 (10)62782510

several independent single-spectrum CT (SECT) scans, i.e. these MECT systems requires as more as energy number times data as SECT. Many researchers have noticed that there is data redundancy in such a MECT scan strategy.[9–11] For example, images at different energy spectra share the same or similar structure information because they are of the same object.[12] This redundancy motivates us to find a new approach requiring less data for spectral image reconstruction. MECT of less data can benefit us very much. Firstly, it provides potential to reduce X-ray dose for patients. Secondly, it can accelerate scan and reconstruction because less data are needed to be acquired and processed. Thirdly, less dose and scanning time help to reduce the cost of MECT.

We have been exploring a multi-arc MECT scanning strategy to decrease the size of projection data. The source/detector pair rotates and samples within a 360° circle so that the quantity of data is roughly equivalent to that in a SECT case. The scanning range is divided into multiple arcs, on which different tube potentials are applied, so each energy X-ray beam might cover only $60° \sim 90°$ angle, i.e. a limited angle CT scan.

Reducing the MECT scanning data raises big challenges. The most difficult one is to recover an image of good quality from incomplete data. According to the data sufficient condition ,[13,14] A fan-beam CT usually requires projection data over an angular range of 180° plus the fan angle of FOV coverage, but the data acquired using our multi-arc MECT approach covers angle far below the requirement. Consequently, the reconstruction suffers severe leakage artifacts caused by limited angular coverage. Some papers [15,16] uses compressed sensing to mitigate the artifacts, but those methods are less applicable to such a severe limited angle problem from our trying.

To combat the heavy limited angle artifacts, we leverage the structure coherence of the sampling data at different energies and jointly reconstruct the imaging using all the data instead of reconstructing the image scanned at each energy independently. Specifically, we first reconstruct a prior image by concatenating all projection data. This prior image is not accurate but roughly reflects the structure information. Then, we divide the image into different parts by $k-$means clustering on the prior image. We assume each cluster represents a local structure in which the pixels share a uniform value within a certain noise tolerance. We combine this prior structure constraint with the $\ell_1-$norm compressed sensing reconstruction to get an overall objective function to be optimized. The spectral image reconstruction is solved by minimizing the overall objective function. The essential of our method is the assumption of uniform distribution within the clustering, which serves the way to keep the structure information among all energy channels. We call this method Joint Clustering Prior and Sparsity Regularization (CPSR).

To summarize, our work has the following contributions,

1. We reduce the coverage angle of each energy to one-third. To our best knowledge, no other work achieves reconstruction given such a severe limited angle problem.
2. We design and implement a reconstruction approach dealing with the limited angle problem by leveraging the coherence among all data at different energies. This approach is compatible with common reconstruction methods.

The rest of the paper is organized as follows. § 2 presents a literature review on the related work. The detailed design of the scanning strategy and the reconstruction algorithm (CPSR) is described in § 3. We evaluate our approach with numerical simulations in § 4. § 5 concludes our work.

## 2. RELATED WORK

Our work is a further study of the multi-energy CT imaging strategy proposed by Shen *et al.*[17] We extends the idea of the SegMECT with modifications on view distribution to make it easier to implement in reality. We also inherit the idea of prior structure image from Shen's work, but apply a new way to process the prior structure image. A stronger structural constraint is exerted on reconstruction by clustering so that we can achieve better performance under a severe limited-angle situation. In our study, the angular coverage of each energy can reach less than 90°.

Compressed sensing has been widely used in CT reconstruction. Two main approaches are sparsity and low rank constraints. The sparsity constraint reduces the data requirement by excavating the sparsity of an image

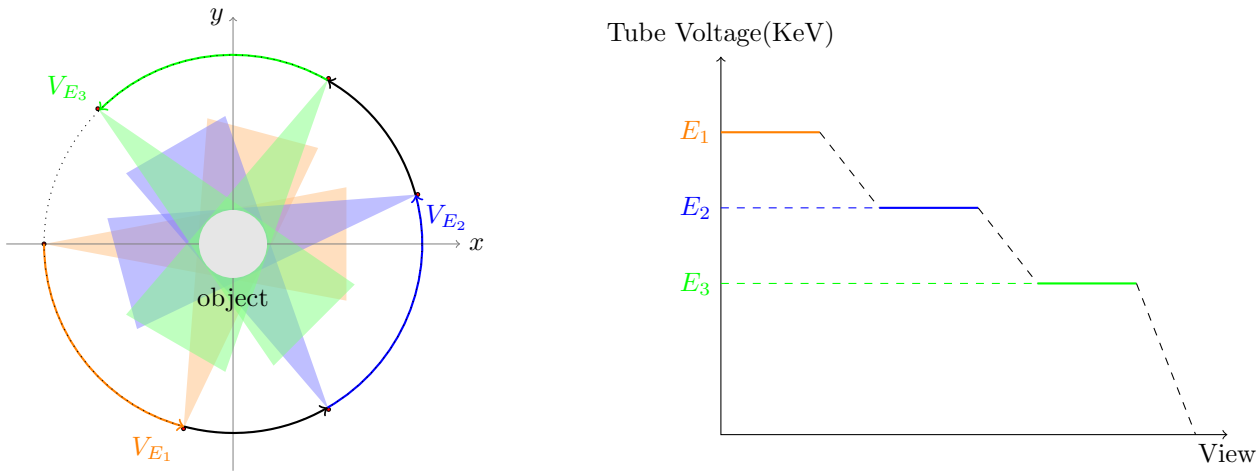


(a) Scanning trajectory

(b) Voltage switching

Figure 1: Scanning strategy

in a single energy channel while the low rank constraint tries to jointly decrease the overall data requirement by exploring the coherence among the images in different energy channels. Sidky *et al*[15,18] developed a novel reconstruction method combining the simultaneous algebraic reconstruction technique (SART) with the total variation regularization. H. Gao *et al*[9] explored the coherence of images from multi-energy channels and proposed a joint sparsity and low rank constraint model. These approaches perform quite well for few-view problems and limited angle problems with relatively simple structures. Our reconstruction algorithm also incorporates a sparsity regularization term to reduce the views of projection.

Some work tries to solve the limited-angle problem by improving the constraints. X. Jin[16] proposed the an-isotropic total variation (ATV) based on the common total variation (TV). Different from TV, ATV adds a stronger sparsity constraint on the directions along which the projection data is absent, thus recovering part of the information corrupted by the limited-angle artifacts. However, this method is not very effective if artifacts are too serious in less than 90° limited-angle cases.

Our work is also related to the sparse dictionary learning reconstruction methods.[19] The dictionary learning approach usually requires a learning procedure before the reconstruction and training images are need to feed the learning algorithm for a satisfactory representative effect. However, no enough training images are available in a lot of cases. Different from those learning-based method to construct the dictionary, we construct the dictionary by clustering a prior image, which makes our algorithm easy to implement.

## 3. METHODOLOGY

### 3.1 Angular sampling Strategy for a spectral CT scan

We design a scanning strategy (Figure 1) by extending the idea of SegMECT.[17] The scanning orbit is segmented into $N_E$ arcs and on these arcs X-ray beams at different energies are used to image an object. Only one source/detector pair without fast-kVp-switching is required. The source potential is tunable. Let $\theta_l, l = 1, 2, \ldots, N_E$ denote the view angles covered by a certain tube potential $E_l$. Generally speaking, the sufficient condition to obtain a good reconstruction is $\theta_l > 180°+$ fan angle, $l = 1, 2, \ldots, N_E$, but with our method the requirement can be relaxed to $\sum_{l=1}^{N_E} \theta_l > 180°+$ the fan angle.

### 3.2 Reconstruction Algorithm

In our notation, we use $N$ to denote the dimension of the image space and $M_l$ the dimension of the projection space for $l^{\text{th}}$ energy channel. Let $\boldsymbol{H}_l \in \mathcal{R}^{M_l \times N}, \boldsymbol{\mu}_l \in \mathcal{R}_+^N, \boldsymbol{p}_l \in \mathcal{R}^{M_l}$ denote the system matrix, linear attenuation

map (image) and projection data at energy $E_l$, respectively. The basic projection model can be formulated as

$$\boldsymbol{H}_l\boldsymbol{\mu}_l = \boldsymbol{p}_l, \quad l = 1, 2, \ldots, N_E \tag{1}$$

Independently solving Eq. 1 will definitely result in severe limited-angle artifacts. To avoid these artifacts we firstly combine the data from all energies to pre-reconstruct a prior image[17]

$$\boldsymbol{\mu}_p = \arg\min_{\boldsymbol{\mu}>0} \|\boldsymbol{H}\boldsymbol{\mu} - \boldsymbol{p}\|_2^2 \tag{2}$$

where

$$\boldsymbol{H} = \begin{pmatrix} \boldsymbol{H}_1 \\ \boldsymbol{H}_2 \\ \vdots \\ \boldsymbol{H}_{N_E} \end{pmatrix} \qquad \boldsymbol{p} = \begin{pmatrix} \frac{\boldsymbol{p}_1}{\|\boldsymbol{p}_1\|_1} \\ \frac{\boldsymbol{p}_2}{\|\boldsymbol{p}_2\|_1} \\ \vdots \\ \frac{\boldsymbol{p}_{N_E}}{\|\boldsymbol{p}_{N_E}\|_1} \end{pmatrix} \tag{3}$$

Although each $\boldsymbol{H}_l$ is ill-conditioned, the combination $\boldsymbol{H}$ of them is not ill-conditioned. With the prior image $\boldsymbol{\mu}_p(x, y)$, we extract the coordinates of the pixels $(x, y)$. The x-coordinate, y-coordinate and the prior pixel value form three features $(x, y, \mu(x, y))$. We use $X$ to represent one feature with $\langle X\rangle$ and $\sigma_X$ being its mean and standard deviation respectively. To use these feature for clustering, we firstly standardize these quantities

$$\breve{X} \leftarrow \frac{X - \langle X\rangle}{\sigma_X} \tag{4}$$

so that Euclidian distances are calculated fairly for comparison. We take each pixel in the prior image as one sample with standardized features $(x, y, \mu)$ and perform $k$-means clustering[20] on the set of all pixels. After the clustering, the prior image is divided into $k$ regions

$$\Omega_c = \{(x, y) \mid \omega(x, y) = \omega_c\}, c = 1, 2, \ldots, k \tag{5}$$

where $\omega(x, y)$ is the cluster label of $(x, y)$ , $\omega_c$ the label of the region $\Omega_c$, and $k$ the number of clusters.

Assuming all the pixels in a region $\Omega_c$ share an identical linear attenuation coefficient within the tolerance of noise, the values of pixels within the region $\Omega_c$ can be represent by one variable $a_c$ and the image $\mu(x, y)$ can be represent by a set of basis functions $\varphi_c(x, y)$,

$$\mu(x, y) = \sum_{c=1}^{k} a_c\varphi_c(x, y) \tag{6}$$

Each element in the basis function is 1 or 0, indicating whether the pixel is in the region $\Omega_c$.

$$\boldsymbol{\mu} = \boldsymbol{\Phi}\boldsymbol{a} = \sum_{c=1}^{k} a_c\boldsymbol{\varphi}_c \tag{7}$$

where $\boldsymbol{\Phi} = (\boldsymbol{\varphi}_1, \boldsymbol{\varphi}_2, \ldots, \boldsymbol{\varphi}_k) \in \mathcal{R}^{N\times k}$ is the dictionary matrix, $\boldsymbol{\varphi}_i$ is a basis vector (element), $\boldsymbol{a} \in \mathcal{R}^k$ the component coefficient. In the dictionary matrix $\boldsymbol{\Phi}$ ($k \ll N$), so the process of clustering constructs a sparse dictionary representation for the image. The sparse dictionary is usually reasonable as there are limited types of materials in an image.

We incorporate the image representation of basis functions by clustering into the common sparse sampling model,

$$\arg\min_{\boldsymbol{\mu}} \frac{1}{2}\|\boldsymbol{H}\boldsymbol{\mu} - \boldsymbol{p}\|_2^2 + \lambda\|W\boldsymbol{\mu}\|_1 \quad s.t. \quad \boldsymbol{\mu} = \boldsymbol{\Phi}\boldsymbol{a} \tag{8}$$

For convenience, we leave out the subindex $l$. All the images at different energies share the same dictionary matrix $\boldsymbol{\Phi}$. $W$ denotes haar wavelet transform and $\|\boldsymbol{W}\boldsymbol{\mu}\|_1$ is our sparse regularization. We refer this reconstruction method as Joint Clustering Prior and Sparsity Regularization (CPSR).

Eq. 8 can be solved by ADMM. Assuming a dummy variable $\boldsymbol{z}$ such that

$$\arg\min_{\boldsymbol{\mu},\boldsymbol{z}} \tfrac{1}{2}\|\boldsymbol{H\mu}-\boldsymbol{p}\|_2^2+\lambda\|\boldsymbol{z}\|_1 \tag{9}$$

$$s.t. \qquad \boldsymbol{\mu}=\boldsymbol{\Phi a},\ \boldsymbol{z}=W\boldsymbol{\mu} \tag{10}$$

The augmented Lagrangian function is

$$L(\boldsymbol{\mu},\boldsymbol{a},\boldsymbol{z},\boldsymbol{y}_1,\boldsymbol{y}_2) = \frac{1}{2}\|\boldsymbol{H\mu}-\boldsymbol{p}\|_2^2+\lambda\|\boldsymbol{z}\|_1+\frac{\rho_1}{2}\|\boldsymbol{\mu}-\boldsymbol{\Phi a}+\boldsymbol{y}_1\|_2^2+\frac{\rho_2}{2}\|\boldsymbol{z}-\boldsymbol{W\mu}+\boldsymbol{y}_2\|_2^2 \tag{11}$$

The ADMM update formula for Eq. 11 is

$$\boldsymbol{\mu}^{(i+1)}=\arg\min_{\boldsymbol{\mu}}\|\boldsymbol{H\mu}-\boldsymbol{p}\|_2^2+\rho_1\|\boldsymbol{\mu}-\boldsymbol{\Phi a}^{(i)}+\boldsymbol{y}_1^{(i)}\|_2^2+\rho_2\|\boldsymbol{z}^{(i)}-W\boldsymbol{\mu}+\boldsymbol{y}_2^{(i)}\|_2^2 \tag{12}$$

$$\boldsymbol{a}^{(i+1)}=\arg\min_{\boldsymbol{a}}\|\boldsymbol{\mu}^{(i+1)}-\boldsymbol{\Phi a}+\boldsymbol{y}_1^{(i)}\|_2^2=\boldsymbol{\Phi}^{\dagger}(\boldsymbol{\mu}^{(i+1)}+\boldsymbol{y}_1^{(i)}) \tag{13}$$

$$\boldsymbol{z}^{(i+1)}=\arg\min_{\boldsymbol{z}}\tfrac{\lambda}{\rho_2}\|\boldsymbol{z}\|_1+\tfrac{1}{2}\|\boldsymbol{z}-W\boldsymbol{\mu}^{(i+1)}+\boldsymbol{y}_2^{(i)}\|_2^2 \tag{14}$$

$$\boldsymbol{y}_1^{(i+1)}=\boldsymbol{y}_1^{(i)}+\rho_1(\boldsymbol{\mu}^{(i+1)}-\boldsymbol{\Phi\alpha}^{(i+1)}) \tag{15}$$

$$\boldsymbol{y}_2^{(i+1)}=\boldsymbol{y}_2^{(i)}+\rho_2(\boldsymbol{z}^{(i+1)}-W\boldsymbol{\mu}^{(i+1)}) \tag{16}$$

Eq. 12 can be solved by Conjugate Gradient(CG) Method.[21] Eq. 14 can be solved by soft thresholding

$$\boldsymbol{z}=S_{\lambda/\rho_2}(\boldsymbol{W\mu}^{(i+1)}-\boldsymbol{y}_2^{(i)}) \tag{17}$$

where $S$ is soft thresholding

$$S_\lambda(x)=\frac{x}{|\,x\,|}\max(|\,x\,|-\lambda,0) \tag{18}$$

For the vector $\boldsymbol{W\mu}^{(i+1)}-\boldsymbol{y}_2^{(i)}$, we perform $S$ element-by-element,

$$z_j=S_{\frac{\lambda}{\rho_2}}((\boldsymbol{W\mu})_j^{(i+1)}-y_{2,j}^{(i)}) \tag{19}$$

## 4. EXPERIMENTAL RESULTS

We validate our method by simulated numerical experiments on a dental phantom. Fan-beam projections with slight noise under three X-ray energy spectra (120kVp, 90kVp, 60kVp) as shown in Figure 1 are used. Overall, 320 detectors are aligned on a 300 mm line. The field of view (FOV) is 200 mm ×200 mm. The distance between the source and the center of FOV is 500 mm. The distance from the center of FOV to the linear detector is 300 mm. Angular sampling step is 1°. We start with case I: setting the views of 120 kVp X-ray to be $V_1=[1°,75°]$, the views of 90 kVp X-ray $V_2=[121°,195°]$ and the views of 60 kVp X-ray $V_3=[241°,315°]$. We pre-reconstruct the prior image which contains the structure information using OS-SART with TV regularization. Then we perform $k-$means clustering on the prior image. The number of clustering is set to be $k=100$. In ADMM iteration, the weight of the sparse regularization is $\lambda=0.05$, the weight of two Lagrangian terms are $\rho_1=0.5$, $\rho_2=1$. Haar wavelet transform of three levels is used. The maximum number of iterations is $N=300$ and the stopping criteria is $\frac{\|\boldsymbol{H\mu}-\boldsymbol{p}\|_2}{\|\boldsymbol{p}\|_2}+\frac{\|\boldsymbol{\mu}-\boldsymbol{\Phi a}\|_2}{\|\boldsymbol{\mu}\|_2}+\frac{\|W\boldsymbol{\mu}\|_1}{\|\boldsymbol{\mu}\|_1}<10^{-3}$.

For comparison, we perform independent reconstruction for each energy channel using OS-SART[22] + TV[15] on complete data and limited-angle data. Projection data in each view form a subset, the maximum number of OS-SART iteration is again $N=300$ and the relaxation factor is $\lambda=0.8$. In each epoch, 20 TV gradient descent iterations are applied with descent speed $\alpha=0.1$. The stopping criteria is $\frac{\|\boldsymbol{\mu}^{(i)}-\boldsymbol{\mu}^{(i-1)}\|}{\|\boldsymbol{\mu}^{(i-1)}\|}<10^{-5}$. Figure 2a shows the prior image and Figure 2b is the resulted cluster image. The reconstruction results are shown in Figure 3. From the left to right are reconstructions by complete data (reference), independent OS-SART+TV reconstruction and CPSR. From the upper to bottom are three different energy channels.

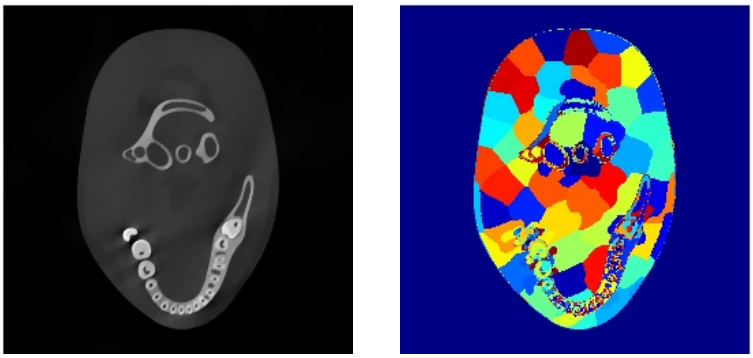

(a) Structure information for prior (b) Clustering

Figure 2: Prior image

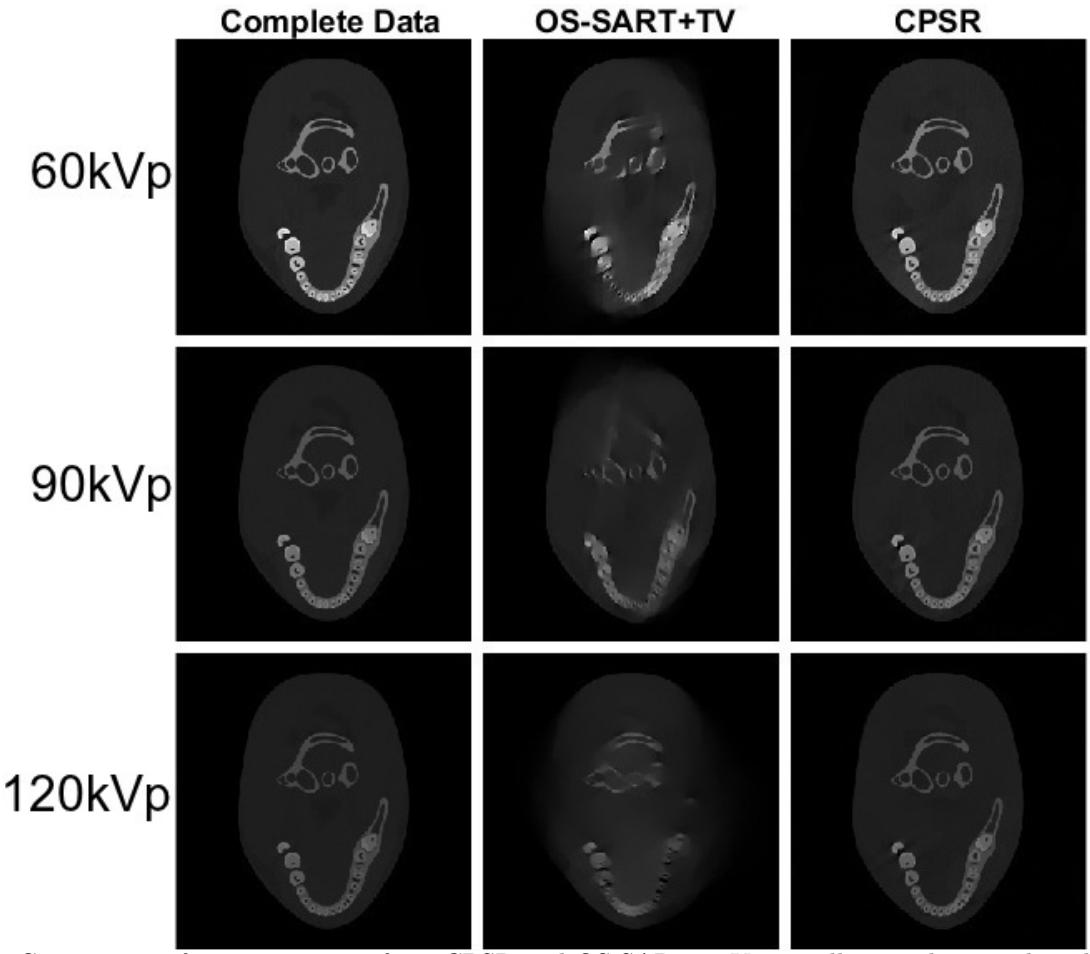


Figure 3: Comparison of reconstructions from CPSR and OS-SART+TV, as well as to the complete data case.

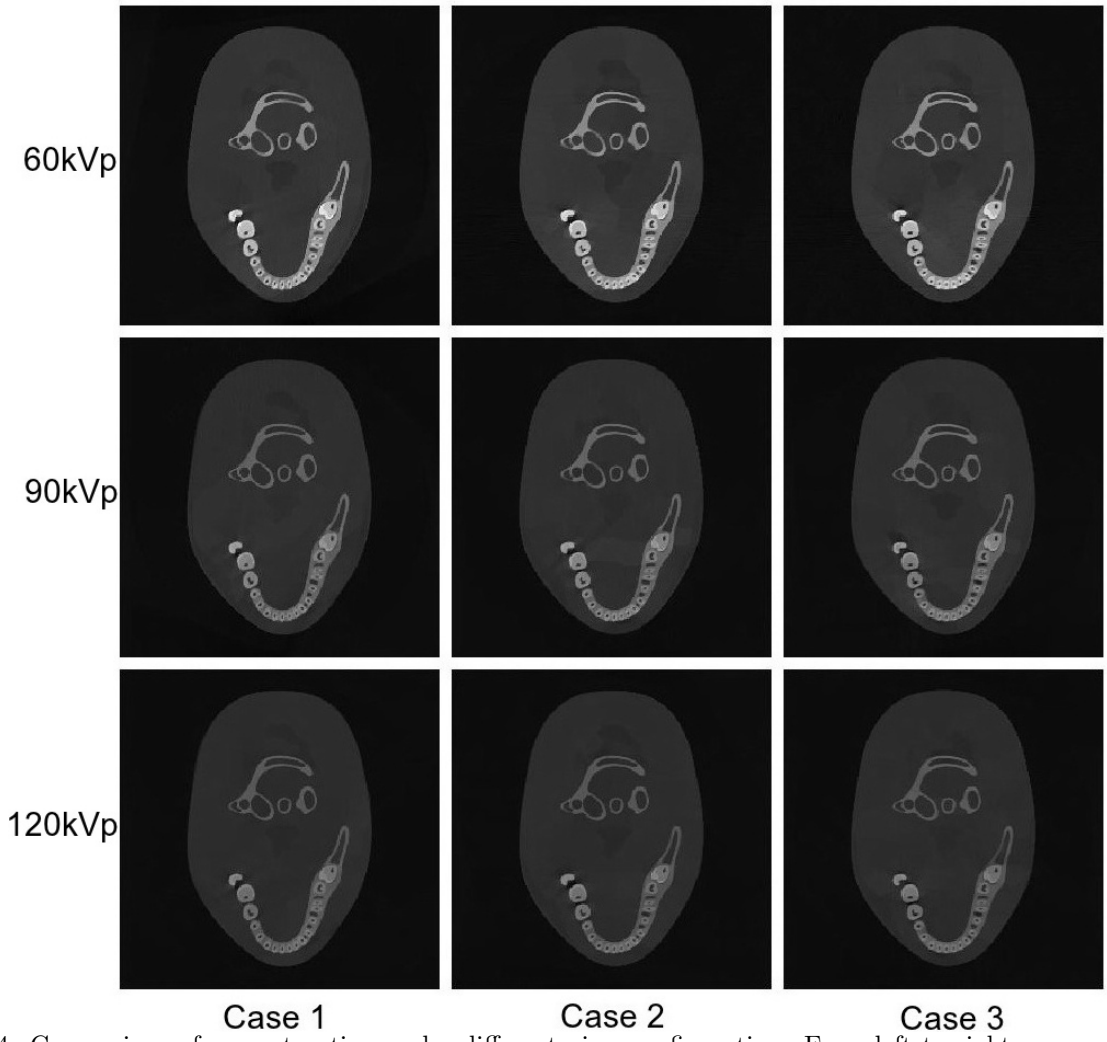


Figure 4: Comparison of reconstruction under different view configuration. From left to right are results from Case I ($V_{120kVp} = [1°, 75°], V_{90kVp} = [121°, 195°], V_{60kVp} = [241°, 315°]$), case II ($V_{120kVp} = [31°, 105°], V_{90kVp} = [151°, 225°]$, $V_{60kVp} = [271°, 345°]$) and case III ($V_{120kVp} = [61°, 135°], V_{90kVp} = [181°, 255°]$, $V_{60kVp} = [301°, 375°]$).

We can see from these reconstructions that the proposed CPSR method is almost totally free from limited-angle artifacts and keeps the edge details well. There is no energy leakage in the images reconstructed by CPSR, while this leakage is obvious using the SART+TV compress sensing approach. The CSPR results recover all structures of teeth and soft tissues, which is greatly impaired by the limited-angle problem in OS-SART+TV reconstruction. From our insight, the CPSR exerts a strong constraint that the pixels share an identical value within a clustering region, which usually represents a local structure of the object (Figure 2b).

To evaluate the robustness of our method at different sampling views. We examine two different sampling configurations (Cases II and III) with the sampling views set as ($V_{120kVp} = [31°, 105°], V_{90kVp} = [151°, 225°]$, $V_{60kVp} = [271°, 345°]$) and ($V_{120kVp} = [61°, 135°], V_{90kVp} = [181°, 255°]$, $V_{60kVp} = [301°, 375°]$) respectively. The reconstruction results under these view settings are shown in Figure 4. In all three cases, the teeth and bone structures are preserved. Some differences exist in the soft tissue region. This is because our approach uses the location of the pixel as clustering features so large soft tissue region is divided into different patches, causing discrepancy in soft tissue regions. It is hopeful to correct this discrepancy with advanced clustering method regarding the whole soft tissue region as one cluster.

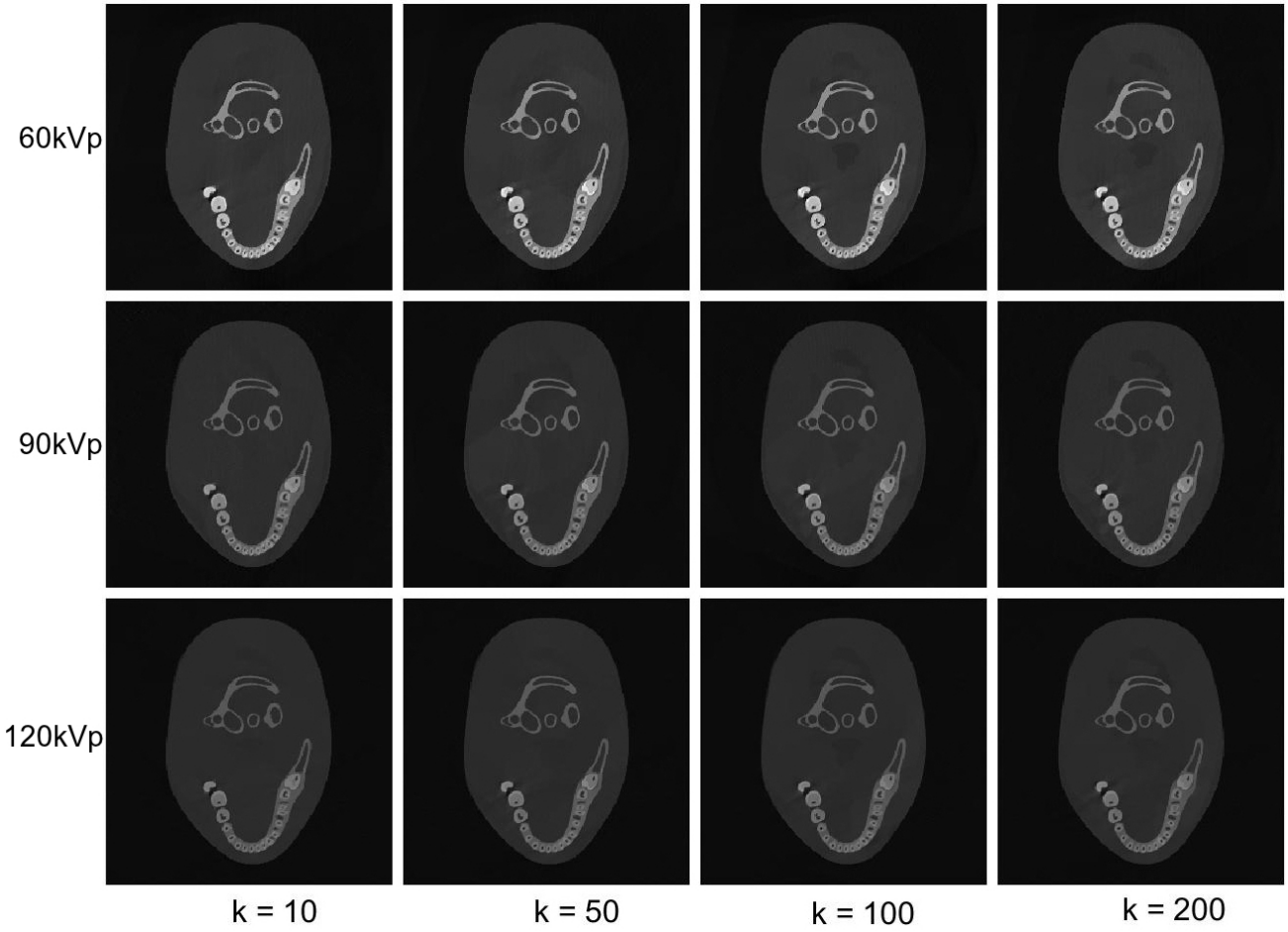

Figure 5: Impact of the number of clusters on reconstruction.From left to right are results from k=10, 50, 100, 200.

To evaluate the robust of our method with different k values, i.e. the number of clusters in the $k$-means clustering approach, we set different k values (10, 50, 100, 200) on the data sampled as case I. The reconstruction results are compared in Figure 5. All the cases preserve the structure information, but the larger $k$ is, the more flexible the approach will be. $k = 10$ works here because the image itself is relatively sparse, can be roughly divided at least into 3 clusters: soft tissue, teeth, and bone. However, given a more complicated image, or a higher requirement on the accuracy of the reconstruction, it is better to set $k$ a larger value.

Considering the prior constraint is very strong and may ruin the reconstruction when the image is not sparse, we combine it with the general OS-SART+TV approach and assign a weight to the prior constraint. This combination brings much flexibility to make the method applicable to more cases. Even if the image is not sparse, we can assign a small weight to the prior constraint and reconstruct an image. In our reconstruction for the tri-energy dental phantom data, we compute the mean value and standard deviation of pixels within each clusters ($k = 100$) (Figure 6). The non-zero standard deviation indicates that our approach can tolerate some variance within each cluster instead of rigidly assigning an identical value for all pixels within the cluster.

## 5. CONCLUSION

We develop an easy-to-implement scanning strategy and a reconstruction algorithm for MECT which can reduce projection views by nearly $N_E$-fold. Our algorithm generates a sparse dictionary representation for the image by clustering a prior image and combines this constraint with a conventional compressed sensing CT reconstruction

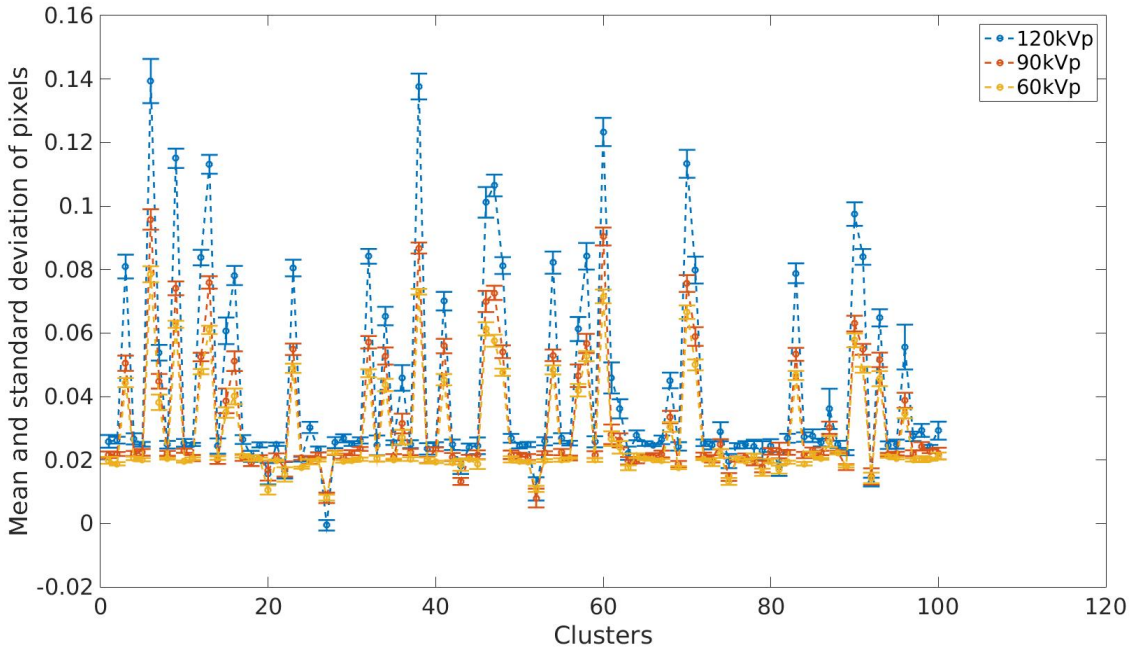


Figure 6: Statistics of final reconstructed images within each cluster.

method. It yields much better performance compared with the independent reconstruction at each energy channel.

## 6. ACKNOWLEDGEMENTS

This work is supported by grants from the National Natural Science Foundation of China (No. 11275104 and 11435007). We would like to thank Le Shen for his support and helpful discussions.

## REFERENCES

[1] Pelc, N., McCollough, C., Yu, L., and Schmidt, T., "We-e-18c-01: Multi-energy ct: Current status and recent innovations," *Medical Physics* **41**(6), 512–513 (2014).

[2] Fornaro, J., Leschka, S., Hibbeln, D., Butler, A., Anderson, N., Pache, G., Scheffel, H., Wildermuth, S., Alkadhi, H., and Stolzmann, P., "Dual-and multi-energy ct: approach to functional imaging," *Insights into imaging* **2**(2), 149–159 (2011).

[3] Xing, Y., Li, Y., and Shen, L., "A general adaptive decomposition method for multi-energy spectral ct," in [*Nuclear Science Symposium and Medical Imaging Conference (NSS/MIC), 2013 IEEE*], 1–4, IEEE (2013).

[4] McCollough, C. H., Leng, S., Yu, L., and Fletcher, J. G., "Dual-and multi-energy ct: Principles, technical approaches, and clinical applications," *Radiology* **276**(3), 637–653 (2015).

[5] Silva, A. C., Morse, B. G., Hara, A. K., Paden, R. G., Hongo, N., and Pavlicek, W., "Dual-energy (spectral) ct: applications in abdominal imaging," *Radiographics* **31**(4), 1031–1046 (2011).

[6] Cormode, D. P., Roessl, E., Thran, A., Skajaa, T., Gordon, R. E., Schlomka, J.-P., Fuster, V., Fisher, E. A., Mulder, W. J., Proksa, R., et al., "Atherosclerotic plaque composition: Analysis with multicolor ct and targeted gold nanoparticles1," *Radiology* (2010).

[7] Shikhaliev, P. M. and Fritz, S. G., "Photon counting spectral ct versus conventional ct: comparative evaluation for breast imaging application," *Physics in medicine and biology* **56**(7), 1905 (2011).

[8] Anderson, N., Butler, A., Scott, N., Cook, N., Butzer, J., Schleich, N., Firsching, M., Grasset, R., De Ruiter, N., Campbell, M., et al., "Spectroscopic (multi-energy) ct distinguishes iodine and barium contrast material in mice," *European radiology* **20**(9), 2126–2134 (2010).

[9] Gao, H., Yu, H., Osher, S., and Wang, G., "Multi-energy ct based on a prior rank, intensity and sparsity model (prism)," *Inverse problems* **27**(11), 115012 (2011).

[10] Shen, L., Xing, Y., and Jin, X., "Structural prior enhanced compressed sensing for ct reconstruction with incomplete data," in [*Nuclear Science Symposium and Medical Imaging Conference (NSS/MIC), 2013 IEEE*], 1–5, IEEE (2013).

[11] Kim, K., Ye, J. C., Worstell, W., Ouyang, J., Rakvongthai, Y., El Fakhri, G., and Li, Q., "Sparse-view spectral ct reconstruction using spectral patch-based low-rank penalty," *Medical Imaging, IEEE Transactions on* **34**(3), 748–760 (2015).

[12] Shen, L., Xing, Y., and Jin, X., "Dual energy ct reconstruction method for incomplete high energy data," in [*Nuclear Science Symposium and Medical Imaging Conference (NSS/MIC), 2013 IEEE*], 1–5, IEEE (2013).

[13] Tuy, H. K., "An inversion formula for cone-beam reconstruction," *SIAM Journal on Applied Mathematics* **43**(3), 546–552 (1983).

[14] Li, L., Kang, K., Chen, Z., Zhang, L., Xing, Y., Yu, H., and Wang, G., "An alternative derivation and description of smith's data sufficiency condition for exact cone-beam reconstruction," *Journal of X-Ray Science and Technology* **16**(1), 43–49 (2008).

[15] Sidky, E. Y., Kao, C.-M., and Pan, X., "Accurate image reconstruction from few-views and limited-angle data in divergent-beam ct," *Journal of X-ray Science and Technology* **14**(2), 119–139 (2006).

[16] Jin, X., Li, L., Chen, Z., Zhang, L., and Xing, Y., "Anisotropic total variation minimization method for limited-angle ct reconstruction," in [*SPIE Optical Engineering+ Applications*], 85061C–85061C, International Society for Optics and Photonics (2012).

[17] Shen, L. and Xing, Y., "Multienergy ct acquisition and reconstruction with a stepped tube potential scan," *Medical physics* **42**(1), 282–296 (2015).

[18] Sidky, E. Y. and Pan, X., "Image reconstruction in circular cone-beam computed tomography by constrained, total-variation minimization," *Physics in Medicine and Biology* **53**(17), 4777 (2008).

[19] Cao, M. and Xing, Y., "Limited angle reconstruction with two dictionaries," in [*Nuclear Science Symposium and Medical Imaging Conference (NSS/MIC), 2013 IEEE*], 1–4, IEEE (2013).

[20] Duda, R. O., Hart, P. E., and Stork, D. G., [*Pattern classification*], John Wiley & Sons (2012).

[21] Hestenes, M. R. and Stiefel, E., "Methods of conjugate gradients for solving linear systems," (1952).

[22] Wang, G. and Jiang, M., "Ordered-subset simultaneous algebraic reconstruction techniques (os-sart)," *Journal of X-ray Science and Technology* **12**(3), 169–177 (2004).